International Journal of Robotics and Automation, Vol. 36, 2021

Special Issue: Automatic Detection and Assessment of Bridge Structures

RESEARCH ON STRESS MONITORING OF CRACKED STEEL BOX GIRDER BASED ON SELF-MAGNETIC FLUX LEAKAGE

Hu Ma,[*,**] Shangkai Liu,[*] Tao Tang,[**] and Runchuan Xia[*]

Abstract

Steel box girder components of long-span bridges inevitably suffer from cracks. The present experimental study of a steel box girder was carried out based on the self-magnetic flux leakage technology. The variation of self-magnetic flux leakage signals during the loading of the cracked steel box girder was obtained, and the influence of the crack size on magnetic flux leakage signals was analysed. It was noticed that the bearing capacity of the steel box girder was affected by cracks and the strain near the crack was larger than those in other areas. The tangential and normal components and the corresponding gradient values of magnetic signals varied with the crack size. The obtained stress and magnetic signal curves manifested a prominent inflection point when the stress was 30–50 MPa. The magnitude of the magnetic signal strength decreased when the stress value exceeded 30–50 MPa. The method was verified to determine the location and size of cracks and the stress state of the steel box girder.

Key Words

Steel box girder, self-magnetic flux leakage, stress monitoring, crack

1. Introduction

Since the first use of a flat steel box girder in the Severn Bridge (a 988-m-long suspension bridge) in 1966 [1], steel box girders have been widely used in long-span bridges due to their advantages of small self-weight, strong spanning ability, and convenient construction [2], [3]. In the contemporary building structure and traffic engineering design, steel box girders are extensively used as compared to concrete box girders [4].

[*] School of Civil Engineering, Chongqing Jiaotong University, Chongqing 400074, China; e-mail: chenxi.bupt@gmail.com, 709278983@qq.com, rcxia@mails.cqjtu.edu.cn

[**] Chongqing Rail Transit (Group) Co., Ltd., Chongqing 401120, China; e-mail: 351472066@qq.com

Corresponding author: Runchuan Xia

Recommended by Dr. Jingzhou Xin

(DOI: 10.2316/J.2021.206-0535)

Steel is the most common material in modern engineering [5] and is susceptible to different direct or indirect damage that causes surface cracks [6]. If cracks in a steel box girder are not detected and processed in time, they can cause serious economic losses and social impacts [7].

Steel box girder cracking accidents have occurred in the Severn Bridge [8] in the UK, the German Haseltal [9], and Sinntal [10] bridges, and other bridges in Japan, the United States, the Netherlands, and France [11]. Since 1970, numerous experimental studies have been carried out to specify the crack design of steel box girders [12], [13]. It is necessary to detect the crack initiation in steel box girders during the bridge operation period [14]. Hence, how to use non-destructive test results for the structural reliability evaluation of steel box girders has become an important research topic [15].

The most commonly used non-destructive test methods for the crack damage evaluation in steel box girders are ultrasonic testing [16], magnetic particle testing [17], eddy current testing [18], penetration testing [19], and the ray detection method [20]. However, these methods have several limitations and cannot efficiently detect cracks in steel box girders [21]. Moreover, conventional detection methods cannot detect the stress concentration of components [22]; therefore, they are not viable for the early diagnosis of cracks [23].

To solve these problems, the self-magnetic flux leakage detection technology has often been used in recent years. This method reveals the intrinsic relationship between the self-magnetic flux leakage signals and structural defect characteristics and achieves early damage detection of steel box girders [24]. The self-magnetic flux leakage detection technology overcomes the shortcomings of traditional non-destructive testing methods and can diagnose the stress concentration zone inside ferromagnetic metal components [25].

In the present research, the location and dimension of cracks in a steel box girder were determined based on self-magnetic flux leakage signals. The steel box girder with cracks was then loaded until it ruptured, and the relationship between stress and self-magnetic flux leakage during the loading process was studied.

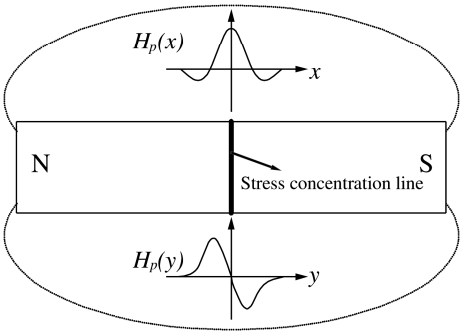

Figure 1. Schematic diagram of self-magnetic flux leakage detection.

2. Self-magnetic Flux Leakage Detection Principle

The self-magnetic flux leakage detection technology is based on the interaction between the working load and the magnetic field of the earth during the operation of a ferromagnetic member. The magnetic domain structure orientation and irreversible reorientation with magnetostrictive properties [26] occur in the stress and deformation concentration region, and the maximum leakage magnetic field H_p is formed. Hence, the tangential component $H_p(x)$ of the magnetic field has the maximum value, whereas the normal component $H_p(y)$ changes the sign and has the zero point (Fig. 1).

The self-magnetic flux leakage detection method works under a combination of magneto-mechanical and magneto-elastic effects [27]. In the magneto-mechanical effect, the change of magnetization is closely related to the change of stress or strain. Under the magnetoelastic effect, when a certain part of an iron workpiece is under a periodic load and an external magnetic field, it experiences the residual magnetic induction strength [28]. Under the conditions of geomagnetism, the magnetic permeability at the defects decreases, and the leakage magnetic field on the workpiece surface increases.

The magnetic dipole model of the magnetic flux leakage field was first proposed in 1966 and the magnetic field of defects was produced by magnetic dipoles of opposite polarities [29], [30]. When the workpiece was subjected to a tensile force, the magnetic flux leakage signal at the stress concentration zone was equivalent to the magnetic flux leakage signal generated by the magnetic dipole [31].

Jiles and Devinc [32] established a theoretical model of the magneto-mechanical effect of ferromagnetic materials under unidirectional stress in 1995. This model indicates that the axial stress can change the internal effective field by magnetostriction and the applied stress can change the internal effective field by the magnetostriction coefficient [33]. Zhang *et al.* applied the self-magnetic flux leakage to an experimental study on the detection of rebar corrosion in concrete [34].

To apply the self-magnetic flux leakage detection to engineering practice, it is necessary to combine the existing health monitoring technology [35] and the damage identification system [36] for research.

3. Experimental Procedure

A combination of artificial pre-set cracks and a static load was used to form cracks in the specific positions of the steel box girder, and subsequently, the static load failure test was carried out. The mechanical model for the static load failure of the steel box girder with cracks was created in a finite element. The stress monitoring of the loading process of the steel box girder with cracks was carried out under self-magnetic flux leakage.

3.1 Test Sample and Test Instrument

3.1.1 Test Sample

A small steel box girder was prepared by welding Q235B steel plates (Fig. 2). It had a length of 1,000 mm, a width of 500 mm, a height of 200 mm, and a top plate thickness of 10 mm. The remaining part of the steel plate was 5-mm thick and was welded symmetrically about 150 mm along the width direction. The bottom of the box girder was 100-mm wide, and the chamfer radius was 100 mm. The steel box girder was prepared by manual tungsten argon arc welding, and the welding material was E50. The box girder consisted of two parts – an upper flat steel plate and a lower non-planar steel plate, and it was processed from the same batch of steel and welded at the laboratory.

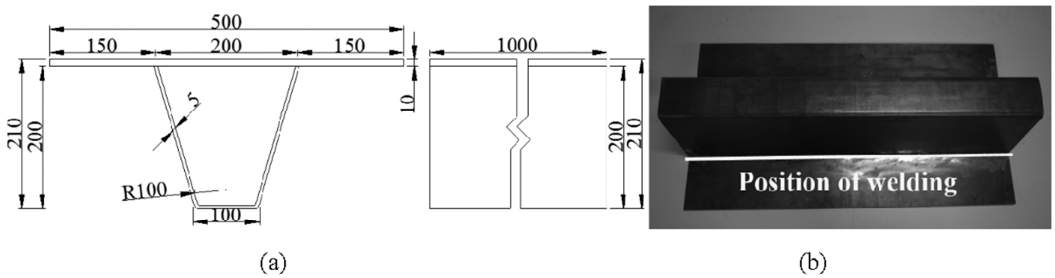

Figure 2. Steel box girder: (a) dimension diagram of the test piece (mm) and (b) physical map of the steel box girder specimen.

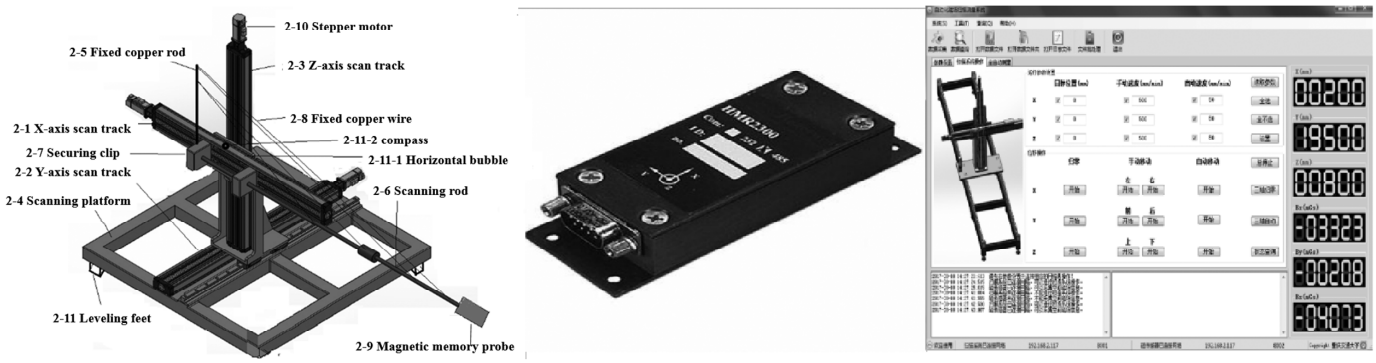

Figure 3. Test device: (a) diagram of the scanning device; (b) HMR2300 three-axis intelligent digital magnetometer; and (c) acquisition program interface.

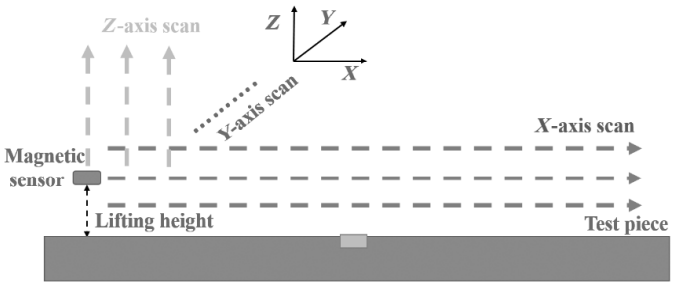

Figure 4. Schematic diagram of scanning.

3.1.2 Test Instrument and Auxiliary System

A self-developed three-dimensional scanning device consisting of a three-dimensional scanning track, a scanning platform, a magnetic memory probe, a stepping motor, and a levelling device was used in this test [Fig. 3(a)].

An HMR2300 three-axis intelligent digital magnetometer (Honeywell International, Morristown, NJ, USA) was used as the magnetic sensor in this experiment [Fig. 3(b)]. The vc2008 software was used to program and develop an automatic acquisition program, and the acquisition frequency was 2 times/s. The program acquisition data interface is displayed in Fig. 3(c).

3.2 Loading Preparation and Test Plan

3.2.1 Magnetic Signal Detection before Loading

(1) Scanning of the steel box girder test piece with no damage
Before processing the test piece, the background magnetic field of the scanning platform and the magnetic induction intensity of the initial leakage magnetic field of the test piece were measured and compared. The magnetic induction intensities B_x, B_y, and B_z recorded by the magnetic memory intelligent scanning device correspond to the sensor probe moving directions X, Y, and Z, respectively. The schematic diagram of sweeping is presented in Fig. 4.

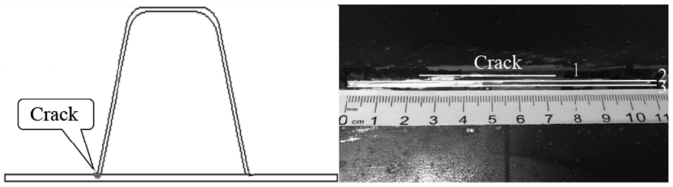

Figure 5. Schematic diagram of crack prefabrication in the steel box girder test piece.

Table 1
Crack Size

Number	Length (cm)	Width (mm)	Depth (mm)
1	5	2	2
2	11	2	2
3	11	2	4

(2) Scanning of the steel box girder specimen after damage
Three macroscopic defects (each lateral spacing was 2 cm, and it increased step by step) were pre-set on the weld position on one side of the steel box girder (denoted as A side) with a hand-held cutter (Fig. 5). These defects were parallel to the weld and simulated the cracks in the steel box girder. The centre of the crack was at the centre of the steel box girder along the length of the weld. Magnetic field scanning was performed to analyse the positions and sizes of the cracks in the steel box girder specimen (Table 1).

3.2.2 Stress and Magnetic Signal Detection during the Loading Process

A jack loading system was used to simulate the applied load with an upper limit of 100 tons. The steel box girder loading diagram and the loading system are displayed in Figs. 6 and 7, respectively. A load pressure sensor was used to control the loading of the jack step by step. Each stage was loaded with the pressure sensor to monitor the change in the appearance of the test piece, and then the

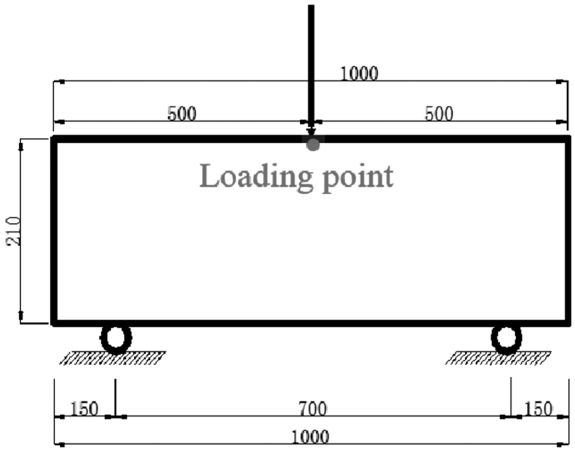

Figure 6. Loading diagram.

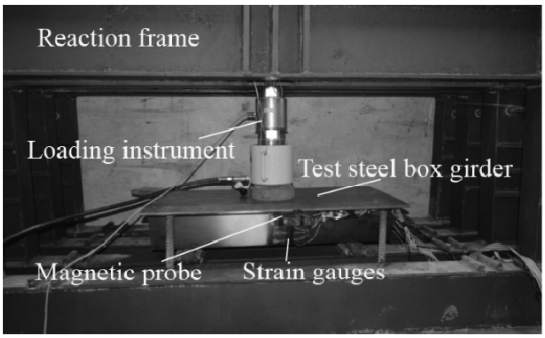

Figure 7. Loading system diagram.

Table 2
Loading Level

Series	Load (kN)	Series	Load (kN)
1	20	6	120
2	40	7	140
3	60	8	160
4	80	9	180
5	100	10	190

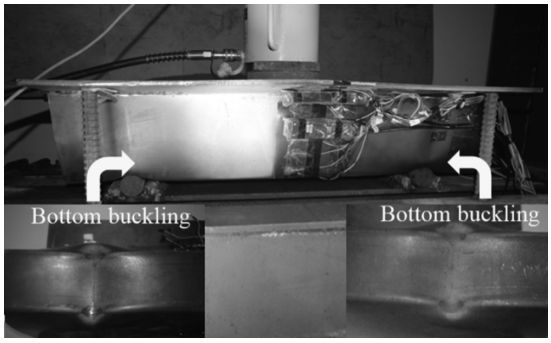

Figure 9. Static load failure diagram of the steel box girder test piece.

next loading stage was started until the test piece was destroyed. The load added by the jack in each stage is presented in Table 2.

The stress test and the magnetic signal strength test were carried out simultaneously. The stress test adopted the traditional paste strain gauge method, and the magnetic signal test used the magnetic sensor monitor mode.

The pre-set crack side of the steel box girder was the A side. Strain gauges were symmetrically attached to the lower edge of the top plate, the web, and the bottom plate. The lower edge of the A-side top plate, the web, and the bottom plate was numbered as A1–A4, A5–A9, and A10, respectively. The strain gauge attachment site is displayed in Fig. 8(a).

Three magnetic signal measuring points (C1, C2, and C3) were arranged in the lower edge of the top plate of the box girder A, the web, and the lower edge of the B-side plate, respectively. The magnetic sensor mounting positions are displayed in Fig. 8(b).

4. Test Results and Analysis

4.1 Stress Analysis of the Steel Box Girder with Cracks

When a load of 100 kN was added to the jack, local buckling occurred at the contact between the steel box girder test piece support and the bottom plate and also at the top plate loading position. When a load of 190 kN was added to the jack, the local deformations of the test piece support and the bottom plate were too large to continue loading (Fig. 9).

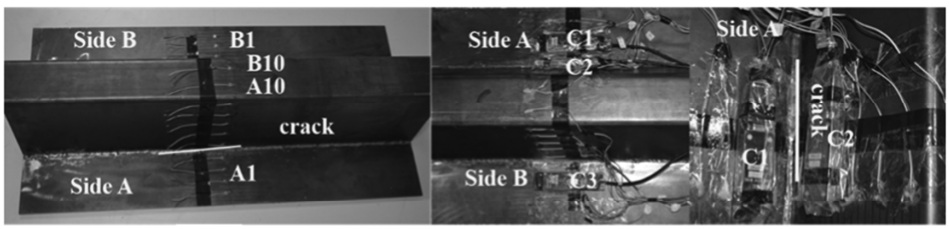

(a) (b)

Figure 8. Sensor layout: (a) strain gauge attachment diagram and (b) magnetic sensor layout.

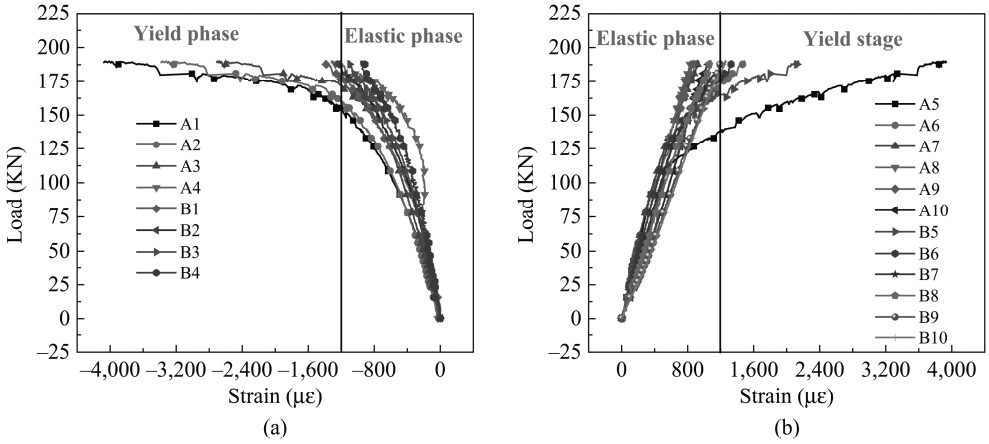

Figure 10. Specimen load–strain curves: (a) compression zone and (b) tension zone.

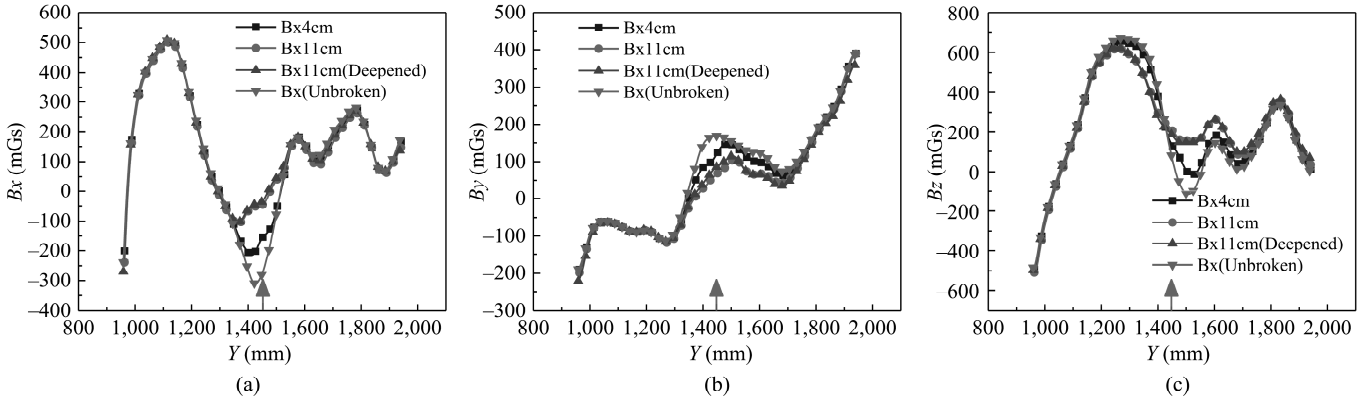

Figure 11. Distribution of scanning magnetic flux leakage signals in the Y-direction: (a) variation of $B_x - Y$ signals; (b) variation of $B_y - Y$ signals; and (c) variation of $B_z - Y$ signals.

The detected strain values at the measuring points during the loading process were analysed, and the corresponding load–strain curves in the compression zone and the tension zone were plotted (Fig. 10).

It is evident that the time of entering the yielding stage in A and B sides was different, resulting in an uneven force on both sides and early failure on one side, and this phenomenon weakened the overall bearing capacity of the steel box girder.

4.2 Magnetic Signal Analysis of the Unloaded Steel Box Girder

The bottom of the steel box girder with cracks was placed horizontally on the fixed area of the test platform ($X = 255$ mm, the position of the weld), and the sensor moved in the Y-direction. The scanning area was $Y = 950$–1,950 mm, and the lifting height was 1 cm. The magnetic induction intensities and scan path curves of the three axial leakage magnetic fields are displayed in Fig. 11, where $B_x - Y$ and $B_y - Y$ are the tangential components of the leakage magnetic field scanned along the Y-axis and $B_z - Y$ is the normal component of the leakage magnetic field. The arrow is located at the centre of the crack.

The magnetic sensor was scanned in parallel to the crack length (referred to as the direction of the slit) (Fig. 11). In the vicinity of the crack existence area ($Y = 1{,}400$–$1{,}500$ mm), the tangential components (B_x and B_y) of the magnetic field abruptly changed. The peak appeared at the centre of the crack, and its value increased with the increase of the crack size. The normal component of the leakage magnetic field (B_z) passed through the zero point at the centre of the crack.

To further explore the relationship between the crack size of the steel box girder and the leakage magnetic field components, the original values of the unbroken steel box girder were deducted from the magnetic field components after the formation of the crack. The gradient of the magnetic flux leakage signal along the Y-axis (parallel to the length of the crack) was obtained, and the leakage magnetic field normal component gradient (dB_z/dy) and the leakage magnetic field tangential component gradient (dB_x) were calculated. The relationships between dB_x/dy, dB_y/dy, and Y-axis coordinates are shown in Fig. 12. The arrow refers to the centre position of the crack.

It is clear from Fig. 12 that in the crack existence area ($Y = 1{,}400$–$1{,}500$ mm), the tangential components (B_x and B_y) of the magnetic field after the deduction of

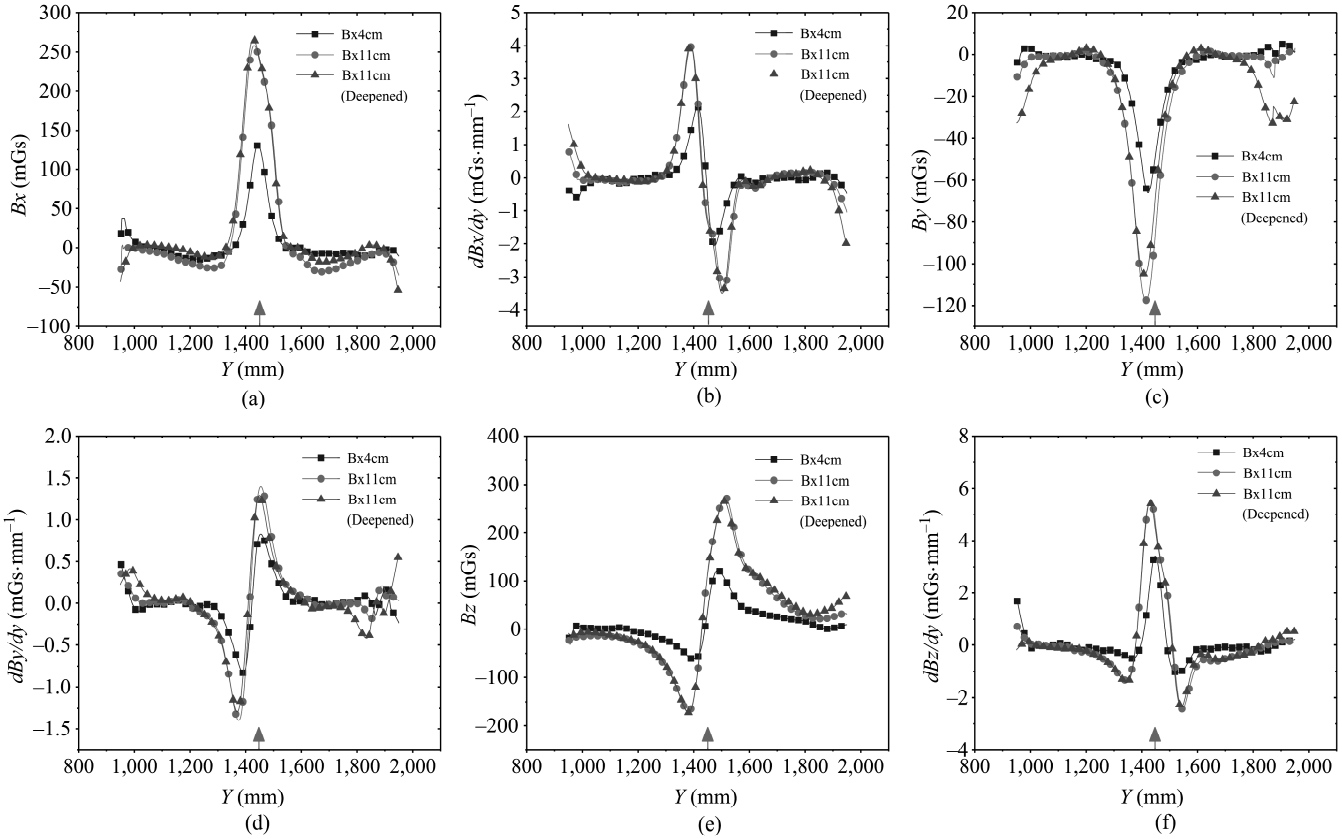

Figure 12. Scanning magnetic flux leakage signals and gradient distributions in the Y-direction: (a) $B_x - Y$ diagram; (b) B_x gradient–Y diagram; (c) $B_y - Y$ diagram; (d) B_y gradient $-Y$ diagram; (e) $B_z - Y$ diagram; and (f) B_z gradient $- Y$diagram.

the original values had a sudden peak. The peak value appeared at the centre of the crack and varied with the crack size. When the crack length increased from 4 to 11 cm, the B_x and B_y peaks became larger. When the crack depth was deepened, the B_x and B_y peak values also increased; however, the change was small.

In the normal component (B_z) of the leakage magnetic field, two opposite peaks appeared in the vicinity of the crack and passed through the zero point at the centre of the crack. The peak value increased with the increase of the crack size. For the leakage magnetic field normal gradient (dB_z/dy), a peak appeared near the centre of the crack, and its value increased with the increase of the crack size, whereas for the tangential gradients of the leakage magnetic field (dB_x/dy and dB_y/dy), two peaks in opposite directions appeared near the crack and passed through the zero point at the centre of the crack. When the crack length increased from 4 to 11 cm, the peak areas of dB_x/dy and dB_y/dy became larger and the peak-to-peak value increased.

4.3 Variation of Magnetic Signals in the Steel Box Girder during Loading

To reveal the relationship between the normal and tangential components of the leakage magnetic field strength and the stress values at the magnetic signal measuring points C1, C2, and C3, the leakage magnetic field strength components and the corresponding stress values are assigned to the vertical axis and the horizontal axis of Fig. 13, respectively.

The magnetic signal measuring point C1 was located in the compression zone under the crack side of the steel box girder. With the increase of the compressive stress, the absolute values of the normal (B_z) and tangential (B_y) components increased. After the compressive stress reached 50 MPa, the absolute values of the normal and tangential components gradually decreased and tended to be gentle. The magnetic signal measuring point C2 was located in the tension zone of the steel box girder web. The absolute values of the normal and tangential components first increased and then decreased, and a prominent inflection point appeared when the tensile stress was 30 MPa. The magnetic signal measuring point C3 was located in the compression zone under the roof of the steel box girder, which always existed in the elastic phase. The absolute values of the normal and tangential components first increased, then decreased, and eventually tended to be flat, and a prominent inflection point was formed when the compressive stress was 40 MPa.

Therefore, the magnitude of the magnetic flux leakage signal first increased with the increase of the stress value; however, when the stress value exceeded a certain point, it decreased with the increasing stress. When the stress was 30–50 MPa, the stress magnetic signal curve had an obvious inflection point, and a very complex non-linear relationship was noticed between magnetization and stress.

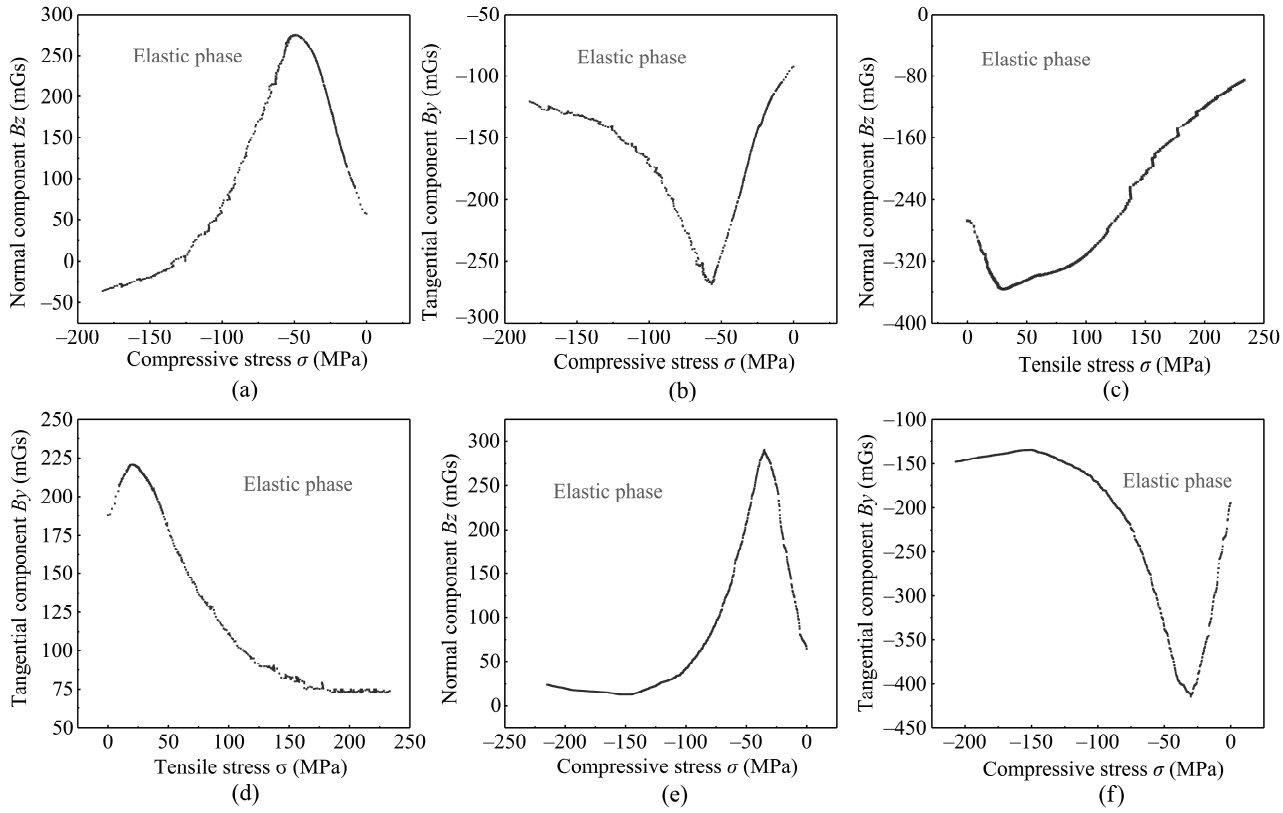

Figure 13. Variation between magnetic signals and stress values at each measuring point: (a) normal component at C1; (b) tangential component at C1; (c) normal component at C2; (d) tangential component at C2; (e) normal component at C3; and (g) tangential component at C3.

The obtained test results were consistent with the findings of the magneto-mechanical theoretical effect model. At the beginning of the elastic phase, the magnetic memory signal weakened the geomagnetic field. To overcome the initial-state instability within a certain loading range, the magnetic memory signal manifested a local enhancement phenomenon. In the later stage of the elastic phase, the external load generated stresses in different parts of the specimen. The stress weakened the magnetic flux leakage signal strength and, finally, approached the hysteresis state; therefore, the magnetic memory signal intensity decreased with the increase of the stress value. As the steel plate at the measurement point of each magnetic signal had just entered the plastic phase, the relationship between the stress and the magnetic signal in the plastic phase was not obvious; hence, the relationship between magnetization and stress at this stage was more complicated.

5. Conclusion

In the present research, the distribution of self-magnetic flux leakage signals in an unloaded steel box girder and the relationship between stress and self-magnetic flux leakage during the loading process of the steel box girder with cracks were studied. The main observations are depicted below.

(1) The bearing capacity of the steel box girder was significantly affected by cracks as an uneven force was generated and the nearby area entered the yielding stage early. The strain increased rapidly after yielding, resulting in an asymmetric deformation of the symmetrical structure, and consequently, the overall load-carrying capacity of the steel box girder was weakened.

(2) Magnetic signals in the steel box girder with cracks of different sizes varied according to the following rules: the tangential component and normal gradient of the leakage magnetic field had a single peak at the centre of the crack, whereas the normal component and the tangential gradient appeared in the vicinity of the crack. Two peaks in opposite directions appeared near the crack and passed through the zero points at the centre of the crack. The peak value increased with the increase of the crack size. With the increase of the crack length, the peak area of the tangential component became larger, and when the crack depth was deepened, the tangential gradient peak area became larger.

(3) Experimental and simulation results revealed that the stress–magnetic signal curve of the steel box girder had a prominent inflection point when the stress was 30–50 MPa; the magnitude of the magnetic signal intensity increased with the increase of the stress value. When the stress value exceeded 30–50 MPa, the magnitude of the magnetic signal intensity decreased with the increasing stress value. In the initial stage of the elastic phase, to overcome the instability of the initial state within a certain loading range, the magnetic memory

signal manifested a local enhancement phenomenon. In the later stage of the elastic phase, the strain generated stresses in different parts of the specimen. The generated stress weakened the magnetic memory signal strength and finally approached the hysteresis state; thus, the magnetic memory signal intensity decreased with the increasing stress value.

Acknowledgement

This research was financially supported by the Technology Innovation and Application Demonstration Project of Chongqing (cstc2018jscx-mszdX0084).

References

[1] K. Brzeziezi and A. Szychowski, Stability and resistance of steel continuous girders with thin-walled box sections, *Archives of Civil Engineering*, *64*(4), 2018, 123–143.

[2] T. Guo, Z.H. Chen, T. Liu, and D.Z. Han, Time-dependent reliability of strengthened PSC box-girder bridge using phased and incremental static analyses, *Engineering Structures*, *117*, 2016, 358–371.

[3] T. García-Segura, V. Yepes, M.F. Dan, and D.Y. Yang, Lifetime reliability-based optimization of post-tensioned box-girder bridges, *Engineering Structures*, *145*, 2017, 381–391.

[4] B. El-Taly, Retrofitting notch damaged box steel girders with composite materials, *KSCE Journal of Civil Engineering*, *22*(8), 2018, 3003–3014.

[5] S.H. Kim, S.J. Park, J.X. Wu, and J.H. Won, Temperature variation in steel box girders of cable-stayed bridges during construction, *Journal of Constructional Steel Research*, *112*, 2015, 80–92.

[6] K. Lee, B. Andrawes, J. Lim, and H. Kim, A study on overturning failure of horizontally curved single steel box girders, *Engineering Failure Analysis*, *97*, 2018, 20–31.

[7] R.E. Koller, I. Stoecklin, B. Weisse, and G.P. Terrasi, Strengthening of fatigue critical welds of a steel box girder, *Engineering Failure Analysis*, *25*, 2012, 329–345.

[8] G. Long, Y.H. Yang, W.Q. Zhu, and Y.J. Liu, Analysis and handling of upwarping accident of main girder of a steel box girder cable-stayed bridge, *Bridge Construction*, *48*(4), 2018, 113–117.

[9] J.R. Kayser and A.S. Nowak, Capacity loss due to corrosion in steel–girder bridges, *Journal of Structural Engineering*, *115*(6), 2016, 1525–1537.

[10] F. Yan, W. Chen, and Z. Lin, Prediction of fatigue life of welded details in cable-stayed orthotropic steel deck bridges, *Engineering Structures*, *127*, 2016, 344–358.

[11] Y.C. Sung, T.K. Lin, Y.T. Chiu, and K.C. Chang, A bridge safety monitoring system for prestressed composite box-girder bridges with corrugated steel webs based on in-situ loading experiments and a long-term monitoring database, *Engineering Structures*, *126*, 2016, 571–585.

[12] S. Saad-Eldeen, Y. Garbatov, and C. Guedes Soares, Effect of corrosion severity on the ultimate strength of a steel box girder, *Engineering Structures*, *49*, 2013, 560–571.

[13] J.R. Kayser and A.S. Nowak, Capacity loss due to corrosion in steel–girder bridges, *Journal of Structural Engineering*, *115*(6), 2016, 1525–1537.

[14] A. Wahab, M.M.A. Aziz, A. Rahman, and M. Sam, Review on microwave nondestructive testing techniques and its applications in concrete technology, *Construction and Building Materials*, *209*, 2019, 135–146.

[15] K. Yao, L.B. Wu, and Y.S. Wang, Nondestructive evaluation of contact damage of ferromagnetic materials based on metal magnetic memory method, *Experimental Techniques*, *43*(3), 2019, 273–285.

[16] Y. Vasseghian, M. Ahmadi, and M. Joshaghani, Ultrasound assisted ash and sulphur removal from bitumen using column flotation technique: Experimental, RSM and ANN methods in modelling and optimization of process, *Iranian Journal of Science and Technology, Transactions A: Science*, *41*(4), 2016, 1149–1163.

[17] D. Grybos, J.S. Leszczynski, C. Swieboda, and P. Lasak, Properties of Fe-based nanocrystalline magnetic powder cores (MPC) and structure of particle size distribution (PSD), *Journal of Electrical Engineering*, *69*(2), 2018, 163–169.

[18] E. Genin, Z.H. Gao, J.A. Varela, and J. Daniel, Nanoparticles: "Hyper-bright" near-infrared emitting fluorescent organic nanoparticles for single particle tracking, *Advanced Materials*, *26*(14), 2014, 2257.

[19] M.J. Sablik and D.C. Jiles, Coupled magnetoelastic theory of magnetic hysteresis, *IEEE Transactions on Magnetics*, *29*(4), 1993, 2113–2123.

[20] U.D. Annakkage and P.G. McLaren, A current transformer model based on the Jiles–Atherton theory of ferromagnetic hysteresis, *IEEE Transactions on Power Delivery*, *15*(1), 2000, 57–61.

[21] Y.L. Cheuk, Characterization and calibration of on-die termination circuits, *Bioresource Technology*, *101*(3), 2006,716–719.

[22] X.K. Shan, Q.X. Qi, J. Hui, and R.C. Wei, Influence of hole diameter and stress concentration on metal magnetic memory signal, *Journal of Magnetic Materials and Devices*, *47*(1), 2016, 49–53.

[23] D. Wu, Z.T. Liu, X.H. Wang, and L.X. Su, Composite magnetic flux leakage detection method for pipelines using alternating magnetic field excitation, *NDT & E International*, *91*, 2017, 148–155.

[24] S. Gontarz and R. Gumiirt, New approach to the evaluation of the effort state of steel based on magneto-mechanical effects, *Mechanics Research Communications*, *82*, 2017, 14–20.

[25] Z.D. Wang, K. Yao, K. Shen, and T. Huang, Advances and evaluation of metal magnetic memory NDT technique, *Journal of Experimental Mechanics*, *27*(2), 2012, 129–139.

[26] K. Yao, B. Deng, and Z.D Wang, Numerical studies to signal characteristics with the metal magnetic memory-effect in plastically deformed samples, *NDT & E international*, *47*, 2012, 7–17.

[27] L.H. Dong, B.S. Xu, S.Y. Dong, and Q.Z. Chen, Characterisation of stress concentration of ferromagnetic materials by metal magnetic memory testing, *Nondestructive Testing and Evaluation*, *25*(2), 2010, 145–151.

[28] S.Y. Dong, D. Wang, B.S. Xu, and C.L. Shi, Characterizing stress concentration by metal magnetic memory signal of Hp(x), *International Journal of Applied Electromagnetics* and *Mechanics*, *33*(3), 2010, 1219–1223.

[29] Yu.L. Gobov, V.E. Loskutov, and Y.Y. Reutov, A dipole model for magnetic leakage fields created by a circular butt-welded joint, *Russian Journal of Nondestructive Testing*, *41*(9), 2005, 614–618.

[30] H.H. Zhu, D.J Liu, S. Feng, and Q. Pan, Magnetic dipole reconstruction geometry modeling for underground ferromagnetic pipe magnetic abnormal detection, *Computer Measurement* and *Control*, *25*(03), 2017, 201–204.

[31] M.J. Sablik, Finite element simulation of magnetic detection of creep damage at scan welds, *IEEE Transactions on Magnetics*, *32*(5), 1996, 4290–4292.

[32] D.C. Jiles and M.K. Devinc, Recent developments in modeling of the stress derivative of magnetization in ferromagnetic materials, *Journal of Applied Physics*, *76*(10), 1994, 7015–7017.

[33] K. Yamamoto, Magnetization change due to stress change in a constant magnetic field on amorphous ribbons, *Journal of Applied Physics*, *81*(8), 1997, 5796–5798.

[34] H. Zhang, J.T. Zhou, R.Q. Zhao, L. Liao, M. Yang, and R.C. Xia, Experimental study on detection of rebar corrosion in concrete based on metal magnetic memory, *International Journal of Robotics and Automation*, *32*(5), 2017, 530–537.

[35] Z. Chen, X. Zhou, X. Wang, L. Dong, and Y. Qian, Deployment of a smart structural health monitoring system for long-span arch bridges: A review and a case study, *Sensors*, *17*(9), 2017, 2151.

[36] J.Y. Yang, B.H. Xia, Z. Chen, T.L. Li, and R. Liu, Vibration-based structural damage identification: a review, *International Journal of Robotics and Automation*, *35*(2), 2020, 921–930.

Biographies

Hu Ma was born in 1979. He received his master's degree in Civil Engineering from Chongqing Jiaotong University in 2015. He works as the Deputy General Manager in Chongqing Rail Transit (Group) Co., Ltd. His current research includes the bridge design and management.

Shangkai Liu was born in 1995. He received his bachelor's degree in Civil Engineering in 2017. He is now studying for a master's degree in Civil Engineering at Chongqing Jiaotong University. His current research includes stress detection and accurate identification.

Tao Tang was born in 1992. He received his master's degree in Architectural and Civil Engineering in 2017, and then he works in Chongqing Rail Transit (Group) Co., Ltd. His current research includes the non-destructive inspection, strengthening, and health monitoring of bridges.

Runchuan Xia was born in 1993. He received his bachelor's degree in Bridge Engineering from Chongqing Jiaotong University in 2015. He is now studying for a Ph.D. in Bridge and Tunnel Engineering in Chongqing Jiaotong University. His current research includes the non-destructive inspection, strengthening, and health monitoring of bridges.